Mannan induces ROS-regulated, IL-17A–dependent psoriasis arthritis-like disease in mice

Ia Khmaladze[a], Tiina Kelkka[b,c,1], Simon Guerard[a], Kajsa Wing[a], Angela Pizzolla[a,2], Amit Saxena[a], Katarina Lundqvist[d], Meirav Holmdahl[d], Kutty Selva Nandakumar[a], and Rikard Holmdahl[a,c,3]

[a]Medical Inflammation Research, Department of Biochemistry and Biophysics, Karolinska Institute, 171 77 Stockholm, Sweden; [b]Turku Doctoral Programme of Biomedical Sciences, 205 20, Turku, Finland; [c]Medical Inflammation Research, Medicity Research Laboratory, University of Turku, 205 20, Turku, Finland; and [d]Department of Clinical Dermatology and Venereology, University Hospital, 221 00 Lund, Sweden

Psoriasis (Ps) and psoriasis arthritis (PsA) are poorly understood common diseases, induced by unknown environmental factors, affecting skin and articular joints. A single i.p. exposure to mannan from *Saccharomyces cerevisiae* induced an acute inflammation in inbred mouse strains resembling human Ps and PsA-like disease, whereas multiple injections induced a relapsing disease. Exacerbation of disease severity was observed in mice deficient for generation of reactive oxygen species (ROS). Interestingly, restoration of ROS production, specifically in macrophages, ameliorated both skin and joint disease. Neutralization of IL-17A, mainly produced by γδ T cells, completely blocked disease symptoms. Furthermore, mice depleted of granulocytes were resistant to disease development. In contrast, certain acute inflammatory mediators (C5, Fcγ receptor III, mast cells, and histamine) and adaptive immune players (αβ T and B cells) were redundant in disease induction. Hence, we propose that mannan-induced activation of macrophages leads to TNF-α secretion and stimulation of local γδ T cells secreting IL-17A. The combined action of activated macrophages and IL-17A produced in situ drives neutrophil infiltration in the epidermis and dermis of the skin, leading to disease manifestations. Thus, our finding suggests a new mechanism triggered by exposure to exogenous microbial components, such as mannan, that can induce and exacerbate Ps and PsA.

autoimmune disease | Ncf1 | animal model

P soriasis (Ps) and psoriasis arthritis (PsA) are chronic, inflammatory diseases. Both genetic and environmental factors contribute to the onset and severity of these disorders. Ps is a skin disease having systemic manifestations (1). Approximately 25% of Ps patients develop PsA phenotypes (2). Genome-wide association studies demonstrate strong disease regulation by the HLA class I region, especially the HLA-Cw6 alleles accounting for up to one-half of the genetic liability to Ps (2–4). Development of arthritis is promoted by additional genes in the class I region: HLA-B38 and HLA-B39 (5). Although the triggers for PsA are not clear, various infections, inflammation-induced stimuli, and physical injuries to the skin (the "Koebner response") were shown to initiate/exacerbate psoriatic lesions (6). *Candida* infections usually lead to different skin pathologies, and increased oral *Candida albicans* infections were reported in patients with Ps (7).

To investigate cutaneous and articular disease pathogenesis, several animal models are used. Some of them reflect the adaptive immune-mediated chronic disease characteristics, whereas others involve innate immune-mediated acute inflammatory responses (8). It was suggested that imiquimod-induced skin inflammation was dependent on the IL-23/IL-17 axis in which plaque-type Ps lesions showed abnormal epidermal proliferation, neoangiogenesis, and accumulation of neutrophils in microabscesses (9). A recent report also emphasized the importance of TNF receptor signaling in keratinocytes for triggering IL-24–dependent Ps-like skin inflammation in mice (10).

Although Ps and PsA were earlier categorized as T helper (Th) 1 cell-mediated diseases, later studies demonstrated the significance of Th17 cells in disease pathology (11, 12). Nishimoto et al. (13) proposed that Th17 cells carrying T-cell receptor (TCR) recognizing epidermal autoantigen could induce IL-17–dependent Ps-like skin inflammation in mice. Of note, an emerging area for the treatment of Ps is to block various components of the IL-17A pathway: IL-23 blockade has clear therapeutic effects, whereas blockers of IL-17A and IL-17R have shown promising results (14).

Here, we found a new inducer of disease lesions and a mechanistic explanation leading to the development of Ps and PsA-like disease in mice. A single i.p. injection of mannan from *Saccharomyces cerevisiae* (i.e., baker's yeast) induced clinical manifestations resembling Ps and PsA in humans, which are characterized by both Ps-like skin lesions (inflamed hyperkeratinous skin) predominantly on the ears and paws and arthritis-like inflammation (swelling and redness) in the articular joints. Similar to models of chronic arthritis (15), inflammation in this disease model was dramatically enhanced in the

Significance

We identified a previously undescribed disease mechanism for psoriasis (Ps) and psoriasis arthritis (PsA)-like disease by developing a new mouse model having characteristic features similar to those of Ps and PsA in human patients. Mannan-induced activation of tissue macrophages triggers IL-17A secretion from γδ T cells, causing Ps-like inflammation. Such inflammation was significantly increased under a reduced oxidative environment. Increased frequency of monocytes/macrophages, depletion experiments, and the disease suppressor function of macrophage-derived reactive oxygen species clearly argue in favor of a role for monocytes/macrophages in this disease model, which is in accordance with the findings in patients with the psoriatic form of skin lesions and arthritis. This novel PsA model could be immensely useful to test new therapeutics for patients with Ps and PsA.

IMMUNOLOGY AND INFLAMMATION

absence of systemic reactive oxygen species (ROS), whereas macrophage-derived ROS was sufficient to suppress the disease severity. We postulate a pathway in which uncontrolled activation of macrophages induces secretion of TNF-α and concurrent activation of γδ T cells in the skin, which lead to local production of IL-17A. This type of activation enhanced the pronounced infiltration of neutrophilic granulocytes. It is possible to block the disease at each of these steps, thus providing potential targets for immunotherapeutic interventions.

Results

ROS Deficiency Exacerbated Mannan-Induced Joint and Skin Inflammation. A single injection of mannan induced joint inflammation and Ps-like skin lesions (Fig. 1 *A* and *B*) in naive inbred mice. This new mouse model has several features of Ps and PsA-like disease. After mannan injection, skin erythema was visible at day 2 on paws (Fig. S1 *A* and *B*) and ears (Fig. 1*C*). Skin plaques appeared from day 3, with the most pronounced skin scaling occurring between days 5 and 6, and part of the scaly skin peeled off later. Joint inflammation started from day 2 onward, at first in the hind paws and spreading to wrists and digits (peak of the disease was around day 3, with a mean maximum score of 12 ± 7 points), but subsided around day 7 (Fig. 1*D*). Arthritis on the front paws was predominantly observed in distal interphalangeal joints, whereas the hind paws developed dactylitis. Conversely, skin lesions (Fig. 1*E*) progressed later and reached maximum disease severity at day 6. From day 7 onward, most of the keratin layer of the affected skin had peeled off. Partial or complete onycholysis (Fig. S1*C*) and alopecia (Fig. S1*D*) on the peeled skin areas were also noted.

The role of phagocyte NADPH oxidase type 2 (NOX2) complex-derived ROS has been previously described as a regulator of chronic inflammation (16). ROS-deficient macrophages are hyperactive and cannot control chronic inflammation, which is dependent on an autocrine mechanism and regulation of interacting T-cell activities, leading to increased severity of arthritis and encephalomyelitis (reviewed in ref. 17). Here, we investigated the role of ROS in Ps-like skin and joint inflammation using B10Q.*Ncf1*^m1j/m1j mice that have a mutation in the *Ncf1* gene (m1j) (the Ncf1 protein also denoted p47phox), and hence reduced ROS production (oxidative burst) (18). As shown in Fig. 1*D*, *Ncf1* mutated mice developed severe joint inflammation within 2 d after mannan injection, which reached the mean maximal disease severity (30 ± 6 points) within 4 d. The frequency of skin lesions was 100%, with more severe cases in B10Q.*Ncf1*^m1j/m1j mice (Fig. 1*E*), whereas B10.Q mice had a significantly milder disease course.

Multiple Exposures to Mannan Induced a Relapsing Disease. Next, we examined the effect of multiple mannan injections in B10Q and B10Q.*Ncf1*^m1j/m1j mice. We boosted mice twice with mannan on days 7 and 14 after disease initiation. Repetitive injections of mannan reproduced the arthritis phenotype, which reached the maximum severity level on days 9 and 17, similar to the first injection (Fig. 1*F*). A more severe disease course was observed in B10Q.*Ncf1*^m1j/m1j mice than in B10Q mice ($P < 0.05$ and $P < 0.01$, respectively). Interestingly, Ps skin scaling returned only after the second mannan injection (on day 16), but the skin peeled off even more quickly than the first time (Fig. 1*G*). Moreover, from day 11 onward, B10Q.*Ncf1*^m1j/m1j mice started to develop pruritus on the body, predominantly on the back and above the eye (Fig. S1*E*). Pruritus was only evident in B10Q.*Ncf1*^m1j/m1j mice, but flaky skin on the tail and alopecia all over the leg was observed in both of the mouse strains. We also observed genetic heterogeneity in disease susceptibility (Fig.
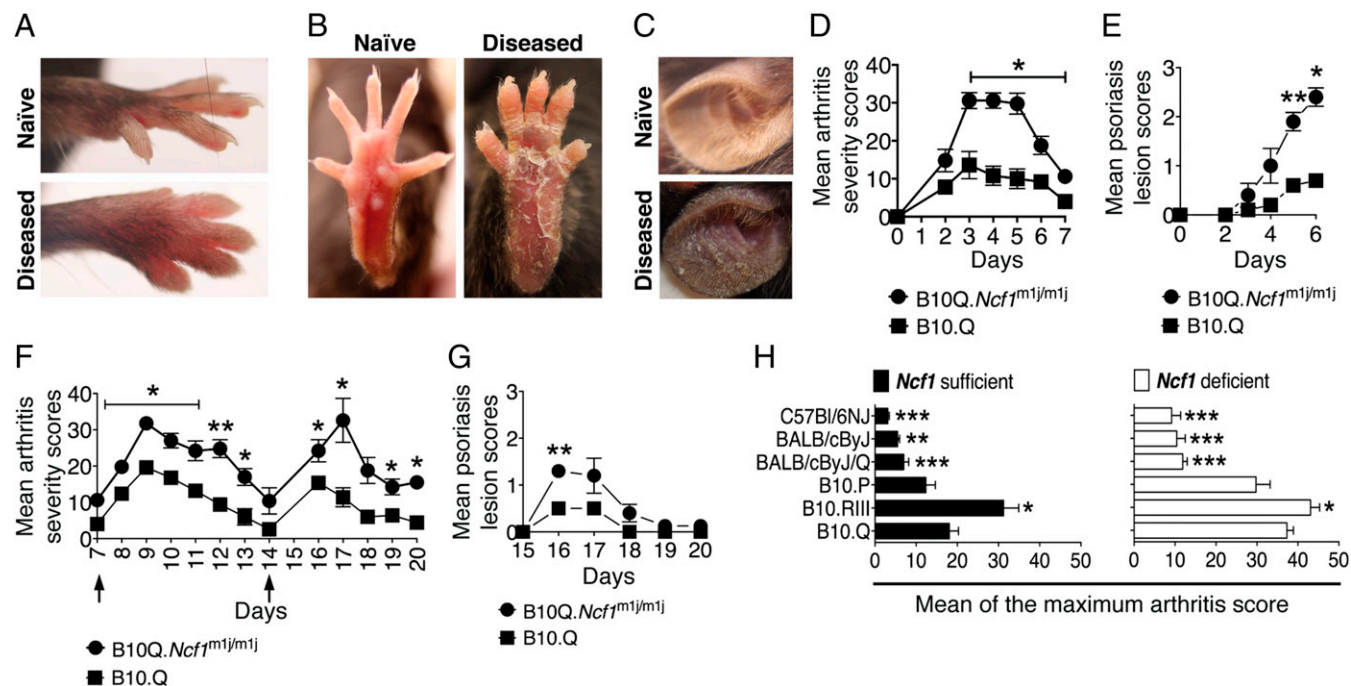

Fig. 1. ROS deficiency enhanced mannan-induced PsA. The arthritic joint phenotype and Ps-like skin lesions in the front (*A*) and hind (*B*) paws of B10Q.*Ncf1*^m1j/m1j mice are shown. (*C*) Ps-like skin scaling in diseased B10Q.*Ncf1*^m1j/m1j mouse ear compared with naive mouse ear. Mean arthritis (*D*) and Ps lesion (*E*) severity in B10Q (*n* = 5) and B10Q.*Ncf1*^m1j/m1j (*n* = 5) mice after a single i.p. mannan injection. Mean arthritis (*F*) and Ps lesion (*G*) severity in B10Q (*n* = 5) and B10Q.*Ncf1*^m1j/m1j (*n* = 5) mice after repetitive mannan injections (days 7 and 14). (*H*) Mannan-induced mean maximum arthritis scores ± SEM in different mouse strains: B10Q (*n* = 8), B10Q.*Ncf1*^m1j/m1j (*n* = 9), B10RIII (*n* = 10), B10RIII.*Ncf1*^m1j/m1j (*n* = 9), B10P (*n* = 3), B10P.*Ncf1*^m1j/m1j (*n* = 9), BALB/cByJ/Q (*n* = 10), BALB/cByJ/Q.*Ncf1*^m1j/m1j (*n* = 8), BALB/cByJ (*n* = 5), BALB/cByJ.*Ncf1*^m1j/m1j (*n* = 7), C57BL/6NJ (*n* = 8), and C57BL/6NJ.*Ncf1*^m1j/m1j (*n* = 7). Significance was calculated by comparing the maximal disease severity of B10Q and B10Q.*Ncf1*^m1j/m1j mice with all of the other strains in their respective groups. *$P < 0.05$; **$P < 0.01$; ***$P < 0.001$.

1H), with the most pronounced disease in B10Q and B10 receptor III (RIII) mice. Of the tested strains, the C57BL/6NJ and BALB/cByJ strains were least susceptible. ROS-deficient mice had significantly more severe disease compared with WT mice in all of the tested genetic backgrounds.

Histological Characterization of PsA Joints. Joint swelling observed in B10Q mice after mannan injection was not due to inflammation, because synovial infiltration and cartilage/bone erosions were clearly absent (Fig. 2A). In contrast, B10Q.$Ncf1^{m1j/m1j}$ mouse joints had synovial hyperplasia, inflammatory infiltrates, and mild cartilage erosions (Fig. 2A). The severity of the disease in B10Q.$Ncf1^{m1j/m1j}$ mice compared with B10Q mice was more pronounced, as confirmed by histopathology scores (Fig. 2B). Moreover, in both mouse strains, entheseal growth was present at the bony insertion of the Achilles tendon (Fig. 2C); additionally, periostitis was observed in B10Q.$Ncf1^{m1j/m1j}$ mice (Fig. 2D).

Histological Characterization of Ps Skin. Histological evaluation of diseased ears in B10Q mice showed cellular hyperplasia, intracorneal pustules, intraepidermal accumulation of neutrophilic granulocytes, and subepidermal inflammatory infiltrates of lymphocytes and neutrophils (Fig. 3A). On the other hand, inflamed ears from ROS-deficient mice had light hyperkeratosis and acanthosis, together with focal parakeratosis and intracorneal

pustules (Fig. 3A). No such pathological signs were observed in naive mice. In addition, altered epidermal keratinocyte differentiation and hyperkeratosis were observed in the diseased hind paw skin tissues of both strains of mice (Fig. 3B). Similar morphological changes were seen in the skin samples of patients who have Ps/eczema, with hyperkeratosis and acanthosis as common characteristics (Fig. S2A).

Mannan-Induced Osteogenic Nodules and Koebner Phenomenon. Male mice had more severe disease than female mice in both of the mouse strains. However, hard nodule-like formations in the wrists were observed in 57% of the female B10Q.$Ncf1^{m1j/m1j}$ mice and 12.5% of the B10.Q mice (a representative image is shown in Fig. 3C) starting from day 11, characterized later as newly formed bone structures (Fig. 3D). In psoriatic patients, de novo psoriatic lesions occur after skin trauma (Koebner response) (19). To test this phenomenon, trauma was induced in one ear by punching the mannan-injected B10Q.$Ncf1^{m1j/m1j}$ mice (Fig. 4E). This injury-induced inflammation was extremely severe, with massive s.c. cell infiltration and elongated/dilated blood vessels in the dermal layer (Fig. 4F).

Redundancy of Adaptive Immunity and Acute Inflammatory Mediators. To investigate the disease mechanisms, we first addressed the contribution of adaptive immunity in this disease process. There was
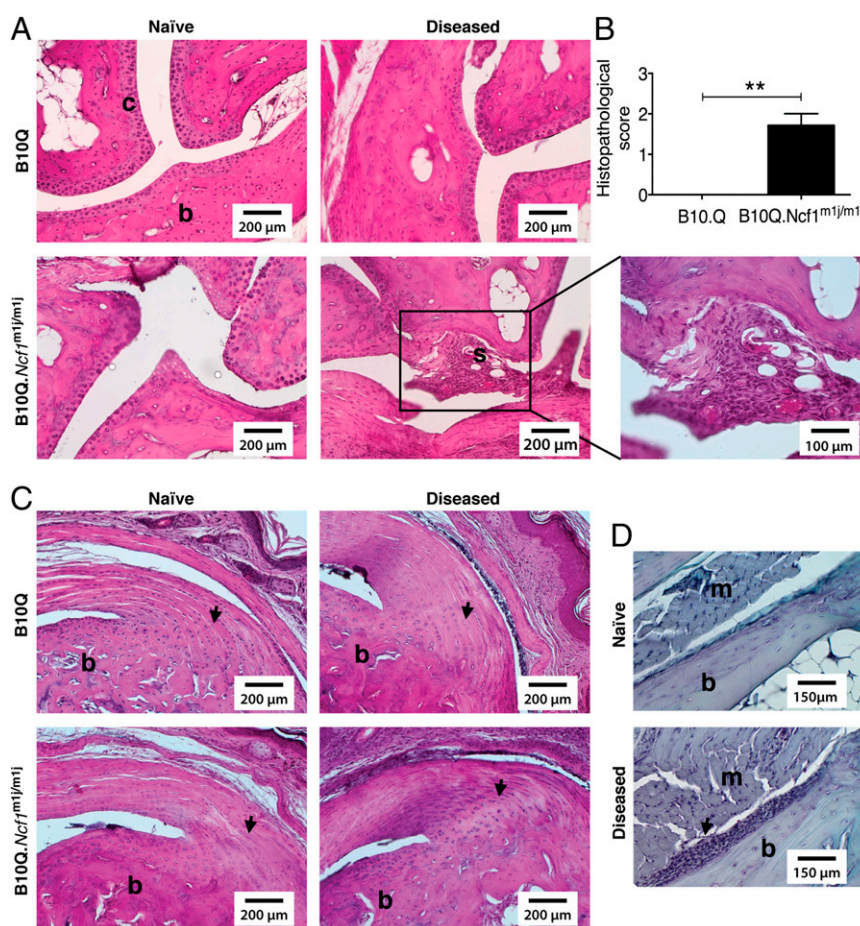
Fig. 2. Histology of mannan-induced articular phenotypes. (A) Representative H&E staining of ankle joints of naive/arthritic B10Q (n = 3–5) and B10Q.$Ncf1^{m1j/m1j}$ (n = 3–5) mice after disease initiation (day 4). Microscopic arthritis was absent in diseased B10Q mice, but B10Q.$Ncf1^{m1j/m1j}$ mice had synovial infiltrates (shown as "s") with mild cartilage damage. (Scale bars: 200 μm. Magnification: 100 μm.) (B) Mean histopathological scores of disease-affected B10Q (n = 5) and B10Q.$Ncf1^{m1j/m1j}$ (n = 7) mouse joints. Data is presented as mean ± SEM. **P < 0.01. (C) Visualization of entheseal inflammation in the Achilles tendon in disease-affected B10Q (n = 5) and B10Q.$Ncf1^{m1j/m1j}$ (n = 7) mice compared with naive mice (arrows). (Scale bars: 200 μm.) (D) Additionally, periostitis was observed in B10Q.$Ncf1^{m1j/m1j}$ mice (n = 7, arrow). (Scale bars: 150 μm.) b, bone; m, muscle; s, synovial membrane.
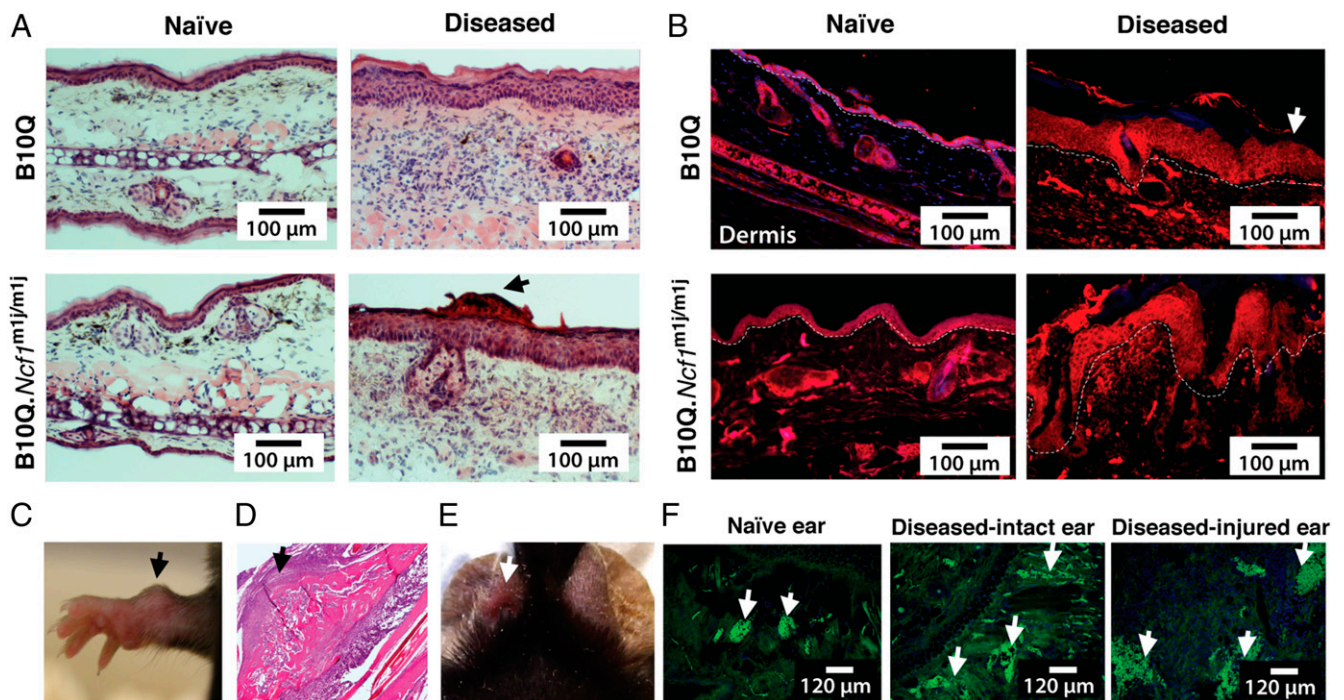
Fig. 3. Mannan-induced cutaneous phenotypes in mice. (*A*) H&E staining of ear tissues from naive and diseased B10Q and B10Q.*Ncf1*^m1j/m1j mice after mannan injection (day 4). (Scale bars: 100 μm.) Dermatitis with intraepidermal accumulation of neutrophilic granulocytes and intracorneal pustules was present in the diseased ears of B10Q mice, whereas mild hyperkeratosis and acanthosis, together with focal parakeratosis and intracorneal pustules (arrow), were observed in the inflamed ears of B10Q.*Ncf1*^m1j/m1j mice. Ears from naive mice did not show any signs of inflammation. (*B*) Involucrin staining (red) showing abnormal keratinocyte differentiation in the hind paw skin sections of mice after disease induction on day 4 (*n* = 3 mice per group). Naive mouse skin contained a normal distribution of epidermal keratinocytes. DAPI was used for staining nuclei. (Scale bars: 100 μm.) The white dashed line indicates the border between the epidermal and dermal layers of the skin (white arrow points toward epidermis). (*C*) Representative image of an "osteogenic nodule" formation (arrow) in a female B10Q.*Ncf1*^m1j/m1j mouse on day 11 after mannan injection. (*D*) H&E staining of an osteogenic nodule illustrates new bone formation (arrow). (Magnification: 10×). (*E*) Representative image of ear punching (white arrow). (*F*) Naive, diseased intact, and diseased-injured ear tissues were stained with MECA-79, depicting dilated blood vessels (arrows) on day 5 after mannan injection (green) (*n* = 3 mice per group). (Scale bars: 120 μm.)

no difference in disease frequency and severity in mannan-injected B10Q.*Ncf1*^m1j/m1j mice with and without functional B cells (Fig. S2*B*). Similarly, αβ T-cell involvement was excluded using αβ TCR-deficient mice with and without functional *Ncf1* expression (Fig. S2*B*). Congenic [complement factor 5 (C5)] and gene [FcγRIII or *NDST*/2 (20)]-deleted mice were used to exclude the role of C5, activating FcγRIII and mast cells in disease initiation (Fig. S2*C*).

Mannan-Induced ROS at the Cellular and Organ Levels. We quantified mannan-induced ROS (reactive oxygen and nitrogen radicals) in vivo using the L-012 probe (21) in the paws of B10Q, B10Q.*Ncf1*^m1j//m1j.*MN*⁺ mice [expressing *Ncf1* in macrophages only (22)] and B10Q.*Ncf1*^m1j/m1j mice (Fig. 4 *A*–*C*). ROS production was significantly increased after mannan injection (Fig. 4*D*) in the paws of B10Q and B10Q.*Ncf1*^m1j//m1j.*MN*⁺ mice compared with the negative controls (B10Q.*Ncf1*^m1j/m1j mice). These data were confirmed at the cellular level in vitro by an oxidative burst assay using a dihydro-rhodamine 123 (DHR-123) probe (Fig. 4*E*). Mannan in the presence of normal mouse serum induced significant ROS production from CD11b⁺ Ly6G⁺ granulocytes, suggesting a requirement for soluble serum components (e.g., natural antibodies, mannose-binding lectin) for triggering phagocytosis-associated mannan-induced ROS production.

Monocyte/Macrophage-Generated ROS Suppressed Clinical Manifestations. To investigate the involvement of CD11b⁺/Ly6G⁻ monocytes/macrophages and CD11b⁺/Ly6G⁺ granulocytes in this disease, flow cytometric analysis was done using cells from epidermal/dermal ear tissues (Fig. 4*F*) and blood samples (Fig. 4*G*) from B10Q.*Ncf1*^m1j/m1j mice (the gating strategy is shown in Fig. S2*D*).

We observed a significant increase in these cell populations (*P* < 0.05, *P* < 0.01, and *P* < 0.001) after mannan injection.

Next, we directly addressed the importance of monocyte/macrophage-produced ROS in disease severity using B10Q.*Ncf1*^m1j/m1j.*MN*⁺ mice, which have monocyte/macrophage-restricted ROS production. As a control group, we included B10Q and B10Q.*Ncf1*^m1j/m1 mice. As shown in Fig. 4*H*, B10Q.*Ncf1*^m1j/m1j.*MN*⁺ mice developed less severe arthritis on days 5–7 after mannan injection (*P* < 0.05 and *P* < 0.01, respectively), demonstrating the disease-suppressing function of macrophage-derived ROS in the latter group.

In addition, to show the significance of monocytes/macrophages and neutrophils in disease pathogenesis, we depleted these cell populations in B10Q.*Ncf1*^m1j/m1j mice using either clodronate liposomes (CLs) (23) or anti-Ly6G antibodies, respectively. The efficiency of in vivo depletion of cells is shown in Fig. S2 *E and F*. Monocyte/macrophage depletion reduced the joint inflammation (Fig. 4*I*) and skin lesions (Fig. 4*J*) (*P* < 0.05 and *P* < 0.01, respectively). Similarly, neutrophil depletion also protected mice from arthritis (Fig. 4*K*) and Ps-like skin lesions (Fig. 4*L*) (*P* < 0.05 and *P* < 0.01, respectively).

Main Source of IL-17A Was γδ T Cells. Further, we investigated the proinflammatory cytokine responses in B10Q.*Ncf1*^m1j/m1j mice after mannan injection. IL-17A was the only cytokine that was increased significantly in the peritoneal cavity [peritoneal exudate cells (PECs)] (Fig. 5*A*). The Th1/Th2 cytokine profile in B10Q.*Ncf1*^m1j/m1j mouse ear skin cell culture supernatant was measured during disease development (days 0 and 2–7) by the cytometric bead array method. Prominent cytokines were IL-17A, IL-4, and
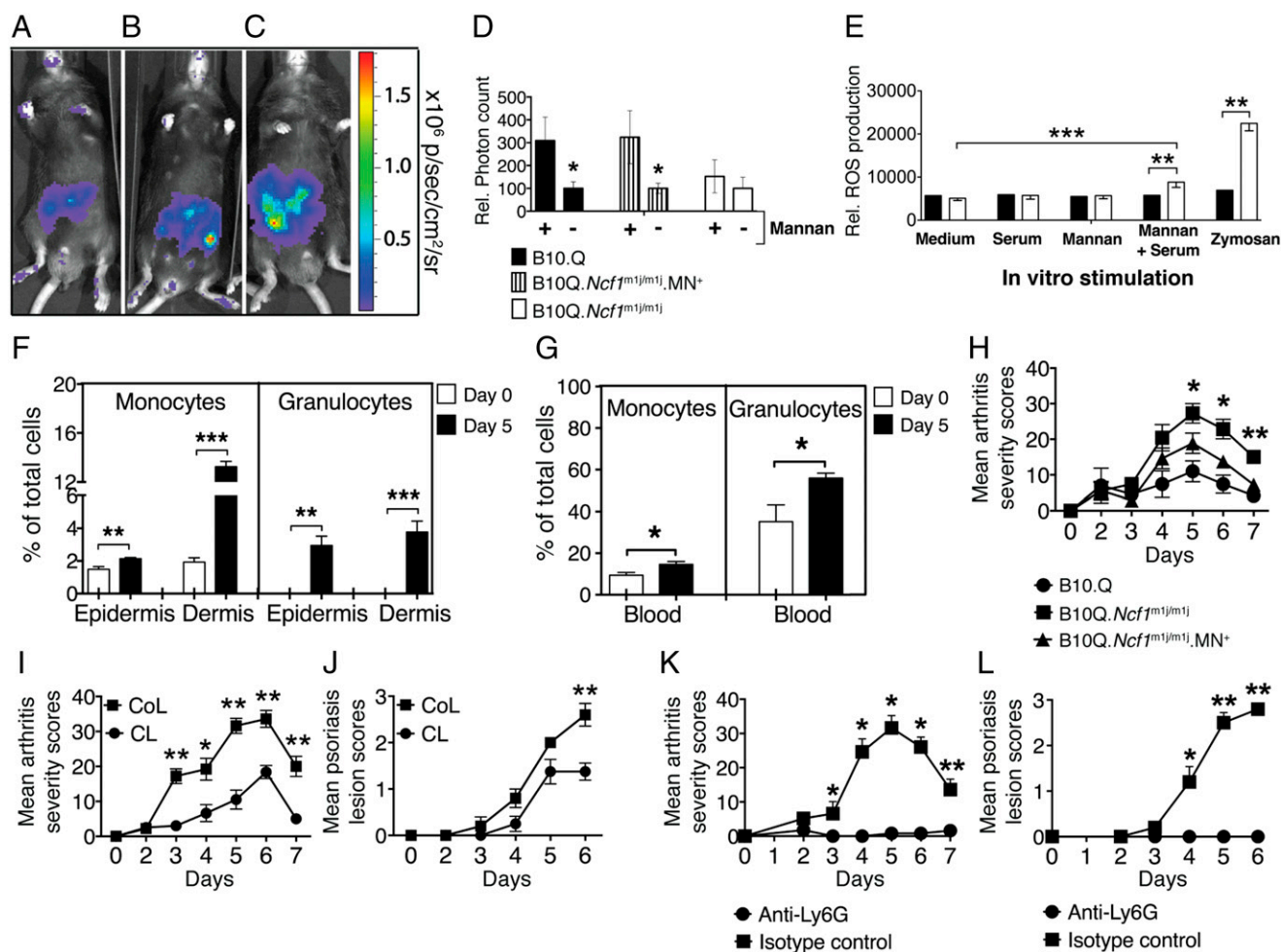
Fig. 4. Contribution of monocytes/macrophages and neutrophils in mannan-induced inflammation. Representative in vivo imaging of ROS with L-012 in B10Q (*A*), B10Q.*Ncf1*^m1j/m1j.*MN*+ (*B*), and B10Q.*Ncf1*^m1j/m1j (*C*) mice. sr, steradian. (*D*) ROS production was measured in the hind paws of B10Q, B10Q.*Ncf1*^m1j/m1j.*MN*+, and B10Q.*Ncf1*^m1j/m1j mice 3 d after mannan injection. Luminescent signal was detected 10 min after L-012 injection. The statistical significance was calculated between naive (designated as −) and mannan-injected (designated as +) mice in all of the experimental groups. Rel., relative. (*E*) In vitro ROS production was measured in blood granulocytes (CD11b+ Ly6G+) of B10Q.*Ncf1*^m1j/m1j (filled bars) (*n* = 4) and B10Q (empty bars) (*n* = 6) mice after 3 h of incubation with stimulants. The total frequency of monocytes/macrophages and granulocytes (flow cytometry gating from single viable cells) in the skin epidermis/dermis (*F*) and blood (*G*) of B10Q.*Ncf1*^m1j/m1j mice on day 0 (empty bars) and day 5 after mannan injection (filled bars) is shown (*n* = 5–7 mice per group). (*H*) Mean arthritis severity in B10Q.*Ncf1*^m1j/m1j (*n* = 7), B10Q.*Ncf1*^m1j/m1j. *MN*+ (*n* = 8), and B10Q mice (*n* = 5). The significance of disease severity was calculated between B10Q.*Ncf1*^m1j/m1j and B10Q.*Ncf1*^m1j/m1j.*MN*+ mice. The mean arthritis (*I*) and Ps skin lesion (*J*) severity of B10Q.*Ncf1*^m1j/m1j mice after macrophage depletion using CLs (*n* = 8 mice/group) is shown. The control group received control liposomes (CoL) only (*n* = 5 mice per group). The mean arthritis (*K*) and Ps skin lesion (*L*) severity in B10Q.*Ncf1*^m1j/m1j mice after neutrophil depletion using anti-Ly6G antibodies is shown. The control group received isotype control antibodies (100 μg per i.v. injection, *n* = 5 mice per group). All of the data are presented as mean ± SEM. *$P < 0.05$; **$P < 0.01$; ***$P < 0.001$.

IL-6, with a maximum concentration of ≥500 ng/mL (Fig. 5*B*), whereas GM-CSF, IFN-γ, IL-5, and TNF-α cytokine concentrations were less than 60 pg/mL (Fig. 5*C*). IL-1α, IL-2, and IL-10 were not detectable. Next, we performed an IL-17A neutralization experiment using B10Q.*Ncf1*^m1j/m1j mice, and, interestingly, both arthritis (Fig. 5*D*) and Ps lesion severity were decreased dramatically (Fig. 5*E*). The efficacy of neutralization was most pronounced between days 2 and 5 for arthritis ($P < 0.001$) and between days 3 and 5 for skin lesions ($P < 0.05$). However, IL-6 neutralization did not affect the clinical outcome (Fig. S3 *A and B*).

To identify the cell subsets responsible for IL-17A secretion, we performed intracellular IL-17A staining in combination with different cell surface markers specific for monocytes/macrophages and γδ T cells. The results demonstrated that IL-17A has originated from γδ T cells (Fig. 5*F*), but not from CD11b+ and F4/80+ monocytes/macrophages (Fig. S3*C*, gating strategy is shown in Fig. S3*D*). We cannot rule out the possibility of αβ T cell–produced IL-17A in this context. However, similar arthritis

disease development in αβ T cell–deficient and -sufficient mice argues in favor of γδ T cells as the main source of IL-17A. Moreover, the frequency of IL-17A+ γδ T cells was significantly increased under a reduced ROS environment in the peritoneal exudates after mannan injection (Fig. S3*E*), which might have contributed to the difference in the disease severity described previously. As a next step, we investigated whether skin γδ T cells had a similar cytokine profile as peritoneal γδ T cells (gating was done as depicted in Fig. S3*D*). As shown in Fig. 5*G*, epidermal and dermal γδ T cells secreting IL-17A were significantly elevated in mice after mannan injection (day 5) compared with preimmunized mouse controls (day 0) ($P < 0.01$ and $P < 0.001$, respectively). A pronounced increase in γδ TCR+ IL-17A+ cell frequencies was observed after in vitro stimulation of the skin cells in mannan-injected mice. Collectively, these data suggest that the main source of IL-17A both in the peritoneum and skin could be γδ T cells. Interestingly, the majority of the γδ TCR+ IL-17A+ cells in both epidermal and dermal skin compartments
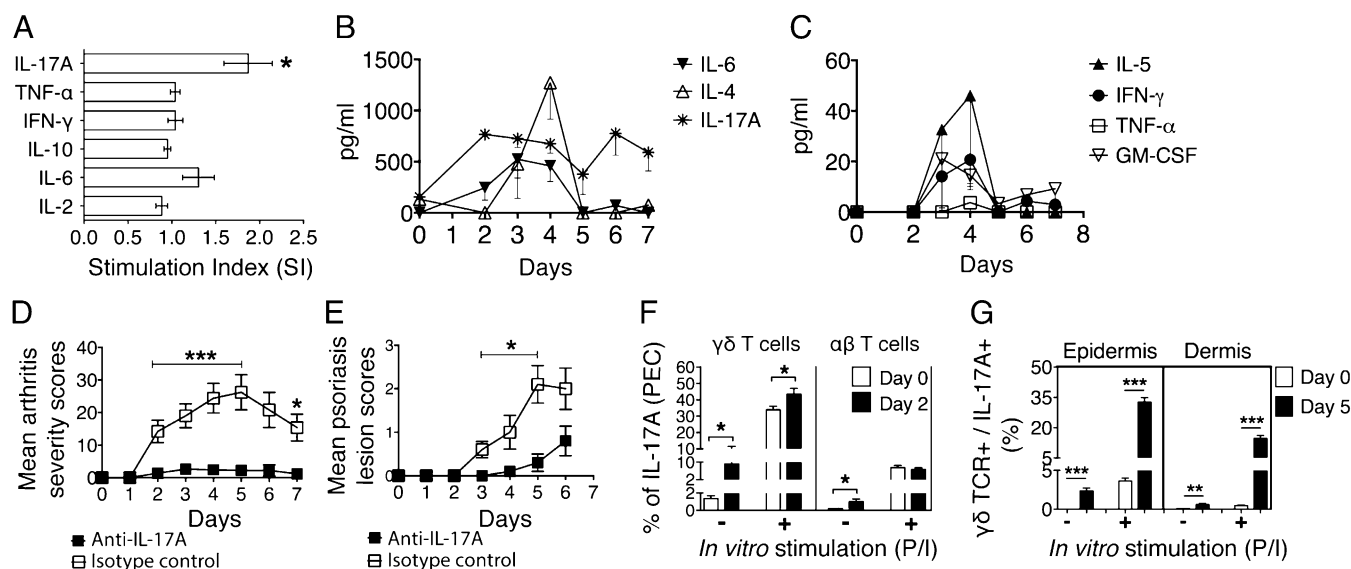
Fig. 5. Mannan-induced inflammation is dependent on γδ T cells secreting IL-17A. (A) Stimulation index (SI) (fold change over naive mice) of different cytokines in the peritoneum of B10Q.Ncf1$^{m1j/m1j}$ mice before (day 0) and after (day 5) mannan injection (n =12 mice per group). The kinetics of cytokine synthesis from the naive (day 0) and mannan-injected (days 2–7) mouse ear skin cell culture supernatant were measured by cytometric bead array (CBA). A total of 1 × 10^6 skin cells were stimulated with PMA/ionomycin and cultured for 4 h at 37 °C in vitro before the assay run (n = 4 mice per time point). (B and C) Cytokine concentration is expressed in picograms per milliliter. Mannan-induced arthritis (D) and Ps lesion (E) severity in B10Q.Ncf1$^{m1j/m1j}$ mice (n = 5 mice per group) treated with anti–IL-17A or isotype control antibody (100 μg per injection). (F) Frequency of PEC-derived IL-17A$^+$ γδ T and IL-17A$^+$ αβ T cells in B10Q. Ncf1$^{m1j/m1j}$ mice before (day 0) and after (day 2) mannan injection (n = 4–8 mice per group). (G) Frequency of IL-17A$^+$ γδ T cells in B10Q.Ncf1$^{m1j/m1j}$ mouse epidermis and dermis before (day 0) and after (day 5) mannan injection (n = 5 mice per group). For in vitro stimulation, PMA/ionomycin (P/I) was used in the culture. All of the data are presented as mean ± SEM. *$P < 0.05$; **$P < 0.01$; ***$P < 0.001$.

were also positive for C-C chemokine receptor 6 (CCR6). In Fig. S3F, we show the frequency of CCR6$^+$ cells gated on γδ TCR$^+$ IL-17A$^+$ cells, which varied between 74% (epidermis) and 64% (dermis) independently after in vitro stimulation.

IL-17A Production Is Dependent on TNF-α. To understand the relation between effector cells (monocytes/macrophages and γδ T cells) and IL-17A, we screened various cytokine stimulants and found that IL-1β and TNF-α were the best candidates for inducing IL-17A production from mannan-activated skin cells (Fig. 6A) and peritoneal cells (Fig. S3G). However, TNF-α, but not IL-1β, neutralization had a profound effect on joint (Fig. 6B and Fig. S3H) and skin inflammation (Fig. 6C and Fig. S3I) ($P < 0.05$). Next, we determined the cellular source of TNF-α. Epidermal and dermal skin cells, gated on CD11b (Low)/Ly6G$^-$ cells and CD11b (Hi)/Ly6G$^-$ cells, defined as monocytes/macrophages, had significantly increased mean fluorescence intensity (geometric mean) for TNF-α (Fig. S3J) at day 5 postdisease induction (Fig. 6D). Remarkably, we could not detect TNF-α positivity in other cell types, including granulocytes (CD11b$^+$/Ly6G$^+$). Neutralization of TNF-α both in vivo and in vitro abrogated increased levels of IL-17A (Fig. 6E), which substantiated our results ($P < 0.01$). Furthermore, TNF-α/IL-23 costimulation of skin cells enhanced IL-17A secretion (Fig. 6F). These data suggest a combination effect of these two cytokines in IL-17A production. However, we failed to detect IL-23 in the diseased skin cell culture supernatants, which leaves the question still open as to whether TNF-α–induced IL-17A is TNF-α–autonomous or regulated via IL-23. In addition, the observed Toll-like receptor 2 (TLR2) expression pattern in CD11b$^+$/CD11c$^-$ cells, CD11b$^+$/CD11c$^+$ cells, and CD45$^+$/γδ TCR$^+$ cells (Fig. 6 G–I) suggests that TLR2 might be the receptor for mannan-induced activation of γδ T cells either directly or via CD11b$^+$ cells for TNF-α synthesis.

Discussion

We developed a new mouse model for Ps and PsA-like disease and identified a new disease mechanism. A single injection of mannan in mice induced an acute disease, and repetitive injections led to a more relapsing disease, resembling Ps and PsA-like symptoms. Interestingly, certain key inflammatory mediators (C5, FcγRIII, mast cells, and histamine) and adaptive immune system players (αβ T or B cells) are redundant in the disease induction process. Macrophage-produced TNF-α triggered γδ T-cell activation and IL-17A production, which, in turn, were involved in recruiting neutrophils to the joints and skin, leading to disease phenotypes. The novel animal model reported herein is under the regulatory control of macrophage-produced ROS.

Ps is an inflammatory skin disease often associated with arthritis (1). Ps may be a high-risk factor for inflammatory arthritis development, because common genetic and environmental triggers result in simultaneous expression of Ps and arthritis. Commensal microbes and infections are suggested as important etiological factors initiating the clinical phenotypes. Yeasts are commonly found in the skin and digestive tract, and individuals with Ps have a higher frequency of oral candidiasis (7). However, whether patients with Ps have an increased occurrence of dermal yeast infections still remains controversial.

Based on the large number of IFN-γ–producing cells found in cutaneous eruptions, Ps and PsA were earlier classified as Th1 cell-mediated diseases, but recent studies suggested a crucial role for Th17 cells (11). Clearly, an immune response to yeast is dependent on Th17 (IL-23/IL-17A) pathway (24). A set of different cytokines, such as TNF-α, IFN-γ, IL-6, and IL-1β, in response to different environmental triggers could induce Th1- and Th17-cell differentiation, and consequently IL-17 induction, which, in turn, stimulates the production of proinflammatory cytokines and angiogenic factors involved in the skin and joint pathologies (25). Current studies also propose that both acquired and innate immunity is involved in the development of PsA.
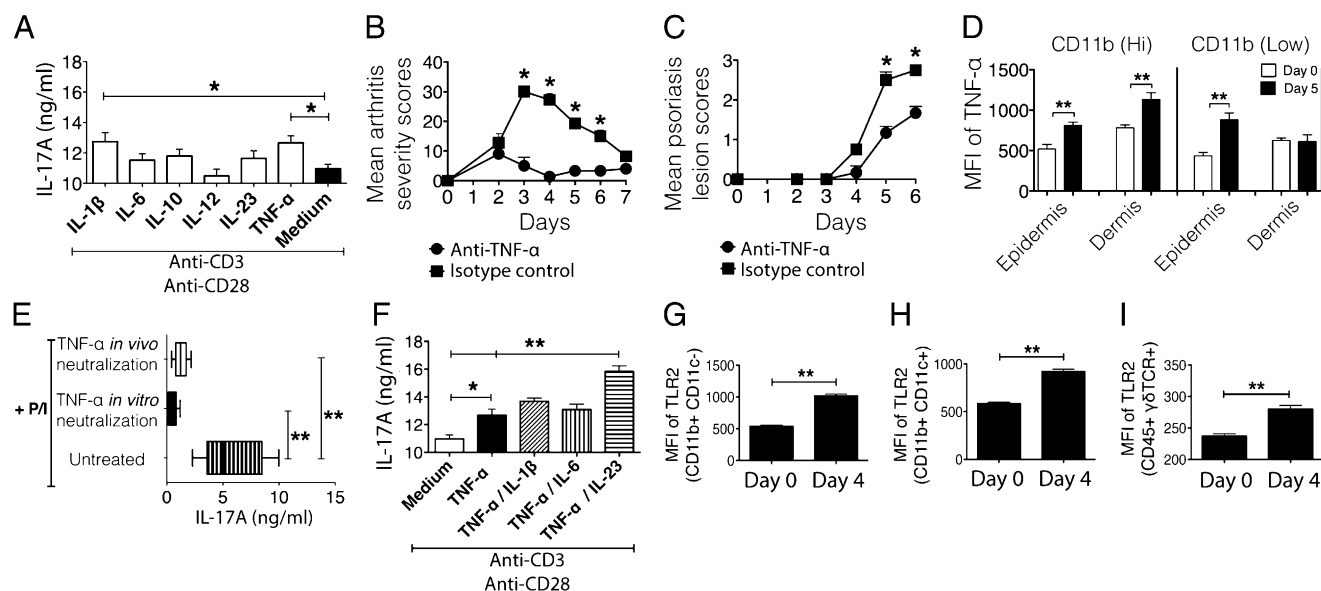
Fig. 6. IL-17A production is dependent on monocyte/macrophage-secreted TNF-α. (A) IL-17A levels (nanograms per milliliter) were measured in epidermal cell culture supernatant on day 5 after mannan injection. Different cytokines were used in combination with plate-bound anti-CD3/CD28 for stimulating cells in culture. The total culture time was 72 h at 37 °C. Mean arthritis (B) and Ps lesion (C) severity in B10Q.Ncf1$^{m1j/m1j}$ mice during TNF-α (n = 3–5 mice per group) in vivo neutralization. (D) Mean fluorescence intensity (MFI; geometric mean) of TNF-α expression in epidermal and dermal CD11b (Low) and CD11b (Hi) cells (gated on Ly6G⁻ cells) after mannan injection. (E) IL-17A levels (nanograms per milliliter) were measured in mannan-activated skin cell culture supernatants (1 × 10^6 cells) stimulated with P/I ± TNF-α neutralization in vivo or in vitro for 48 h. (F) IL-17A levels (nanograms per milliliter) were measured in epidermal cell culture supernatant on day 5 after mannan injection. TNF-α alone and in combination with IL-1β, IL-6, and IL-23 was used, together with plate-bound anti-CD3/CD28 for stimulating cells in culture. The total culture time was 72 h at 37 °C. The MFI (geometric mean) of TLR2 in CD11b⁺ CD11c⁻ (G), CD11b⁺ CD11c⁺ (H), and CD45⁺ γδ TCR⁺ (I) epidermal skin cells before (day 0) and after (day 4) disease induction in B10Q.Ncf1$^{m1j/m1j}$ mice (n = 5 mice per group) is shown. All of the data are presented as mean ± SEM. *P < 0.05; **P < 0.01.

However, the interplay between skin and joint pathologies has been challenging to study, because there are only a very limited number of animal models available that could replicate both organ phenotypes. Epidermal deletion of JunB and c-Jun (26), the absence of endogenous MHC class II (27) in inbred mice, or reduced expression of the common chain of β2 integrin in CD18 hypomorphic PL/J mice (28) led to PsA-like disease symptoms. On the other hand, TLR7 ligation in innate immune cells by imiquimod, triggered Ps symptoms (29), while targeting of intracellular adhesion molecule-1 ameliorated the disease (30).

In the present study, we used mannan as an inducer of joint inflammation and Ps-like skin lesions in the inbred mouse strains. The clinical disease in B10Q mice resembles Ps with erythema and edema (scaly skin on the ears and peripheral joints), with microscopic hyperkeratosis, acanthosis, and inflammatory cell infiltrates, as well as increased dermal vascularity/angiogenesis. However, ROS-deficient B10Q.Ncf1$^{m1j/m1j}$ mice had more severe skin lesions accompanied by arthritis and characterized by enthesitis, synovial hyperplasia with inflammatory cell infiltrates, mild cartilage damage, and periostitis. Onycholysis and alopecia were present during the late phase of the disease. Some of these clinical features were reported as clinical subphenotypes of patients with PsA (31). Moreover, osteogenic nodule formation in the wrists and Koebner phenomenon in injury-induced ear tissue are analogous to the "koebnerized" psoriatic skin observed in patients with Ps who have traumas (32).

ROS is not only a regulator of inflammation (16) but also acts as a suppressor of arthritis and encephalomyelitis (15, 21, 22). Although ROS has been suggested to be pathogenic in Ps and scleroderma (33, 34), reduced neutrophil respiratory burst was observed in patients with scleroderma (34), suggesting a protective role for ROS. Recently, imiquimod-induced psoriatic dermatitis was shown to be prevented by ROS (35). Moreover, phagocyte-produced ROS affects rheumatoid arthritis development (36) and

β1,3-glucan of *Alcaligenes faecalis*-induced ROS from monocytes suppressed innate inflammation (37). In mannan-induced inflammation, ROS deficiency promoted Ps and arthritis, diseases that were suppressed by monocyte/macrophage-derived ROS, similar to collagen-induced arthritis inflammation (22). However, the mechanism whereby ROS protects against Ps and PsA needs to be explored further in detail but is likely to be different in comparison to autoimmune arthritis, in which αβ T cells play a critical role.

Although mannan-induced inflammation in mice resembles human PsA in many aspects, adaptive immunity did not seem to have a major role in affected mice, whereas involvement of both adaptive and innate immunity is recognized in humans (38). Psoriatic lesions contain mast cells (39), and complement activation is suggested to be important in disease mediation in mouse arthritis and patients with Ps (40, 41), whereas the contributions of mast cells, FcγRIII, and C5 in this disease model seem to be redundant. Conversely, increased frequency of monocytes/macrophages, depletion experiments, and the suppressor function of macrophage-derived ROS clearly argue in favor of a role of monocytes/macrophages in the disease, which is in accordance with the findings in patients with the psoriatic form of skin lesions (42, 43) and arthritis (22).

Because we excluded the involvement of adaptive immunity and observed significant reduction of inflammation after IL-17A neutralization, we searched for the source of IL-17A. Alveolar macrophages in allergic lung inflammation (44), Th17 cells in SKG arthritis [a mouse model of a spontaneous arthritis caused by a ζ-chain–associated protein kinase 70 (ZAP-70) mutation] (45), and Rorγt⁺ and γδ T cells invading the skin in psoriasiform plaque formation were reported as cellular sources for IL-17A in mice (46). IL-17 acts on skin keratinocytes to produce innate defense proteins and chemokines promoting inflammation in Ps that was amplified by TNF. Antibodies against IL-17 and its receptor showed outstanding efficacy in phase 2 Ps trials (47).

In the mouse model, i.p. mannan delivery induces systemic activation of the immune system, which led to further activation of IL-17A–producing skin γδ T cells directly or indirectly via monocyte/macrophage-secreted TNF-α through TLR2 stimulation. Of note, *S. cerevisiae* mannan recognition of TLR2 expressed on macrophages has been previously described (48).

In mannan-induced inflammation, γδ T cells present in PECs possibly activated by TNF-α from macrophages are the primary source of IL-17A. The majority of epidermal/dermal γδ T cells secreting IL-17A were expressing CCR6. It is known that IL-17A induces CCL20 expression in keratinocytes, a ligand for CCR6 (49–51), and directs recruitment of CCR6$^+$ cells to psoriatic lesions. Intriguingly, IL-23–induced Ps-like inflammation required CCR6 (52). A proinflammatory subset of γδ T cells (Vγ9Vδ2) producing IL-17A was recently reported to home the skin compartments and activate keratinocytes in patients with Ps (53). It is well known that humans have many fewer γδT cells in the skin than the mouse, but it is likely that a similar function is also carried out by other innate immune cells (46, 54).

Similar to the case in patients with PsA (55), TNF-α neutralization led to alleviation of disease manifestations in mice. IL-17A up-regulates various chemokines (49), which, in turn, are responsible for the recruitment of neutrophils into Ps skin. We observed keratinocyte hyperproliferation and infiltration of neutrophils in the epidermis and dermis. Depletion of neutrophils in vivo reduced disease severity dramatically similar to therapeutic depletion of myeloid lineage leukocytes in patients with generalized pustular Ps (56).

In conclusion, we demonstrate a new pathogenic pathway leading to Ps and PsA-like disease triggered by mannan in susceptible mouse strains. Local activation of macrophages produced TNF-α, which triggered IL-17A secretion from γδ T cells causing local Ps-like inflammation. Such inflammation was significantly increased under a reduced ROS environment but was unaffected by adaptive immune system players (αβ T and B cells) and acute inflammatory mediators (C5, FcγRIII, and histamine). This novel PsA model could be useful for studies of the pathogenesis of Ps and PsA and for the development of new therapeutics.

Materials and Methods

Experimental Animals. BALB/cByJ and C57BL/6NJ mouse strains were from The Jackson Laboratory. Founders of B10Q (C57/Bl10.Q/rhd) and B10P (C57/Bl10. P/rhd) mice were from Jan Klein (Tubingen University, Tubingen, Germany), but they have been maintained by Rikard Holmdahl (rhd). B10.RIII founder mice were originated from the stock of Jan Klein, Tübingen University, Tübingen, Germany. BALB/cByJ/Q mice were generated by introgressing the H-2^q haplotype from B10Q mice into a BALB/c genetic background. A mutation in the *Ncf1* gene (m1j) (the Ncf1 protein also denoted p47phox) in the B10Q mice, designated as B10Q.*Ncf1*$^{m1j/m1j}$, impairs the expression of the *Ncf1* gene, thereby totally blocking the function of the NOX2 complexes, as described earlier (15, 18). The B10Q.*Ncf1*$^{m1j/m1j}$.MN$^+$ strain has a transgene expressing functional *Ncf1* on macrophages using the human CD68 promotor (22, 57). This transgene is used when expressed heterozygously, and MN$^-$ mice are B10Q.*Ncf*$^{m1j/m1j}$ littermate controls.

Deletion of the B-cell receptor μ constant region gene [μMT; from Werner Mueller, University of Cologne, Cologne, Germany, and back-crossed to B10. Q mice (>12N)], the TCR-β gene [from The Jackson Laboratory and back-crossed to B6 (>10N) and an additional 6N to B10Q], and the NDST2 gene (generated in B6 mice; from Gunnar Pejler, Swedish University of Agricultural Sciences, Uppsala, Sweden, and backcrossed 4N to B10Q) (20), and complement C5 congenic mice [B10.Q.NOD-*Cia2* mice (58) backcrossed to B10Q mice (>13N)], resulting in respective deficiency on the B10.Q background, were used. The FcγRIII gene-deleted mice with a B6.129P2 background were from The Jackson Laboratory and were backcrossed 7N to B10Q mice. All of these mice were housed under specific pathogen-free conditions in individual ventilated cages with wood shaving bedding, with a paper napkin as enrichment, and in a climate-controlled environment having a 12-h light/dark cycle. All animal experiments were performed in a controlled way balanced for age and sex, with mixing in cages and use of littermates; the investigators were blinded to the genotype of the mice and the treatment used for each experiment. Regional ethical committees at

Medical Inflammation Research, Karolinska Institutetet, Stockholm, Sweden (N66/10, N169/10), and at Medical Inflammation Research, University of Turku, Turku, Finland (ESHL-2008-02873/ym-23 and ESAVI-497/041003/2011), approved all of the animal experiments. A regional ethical committee in Lund, Sweden (EPN-144/2010, EPN-82/2012), approved the use of all human tissue samples, which were obtained from healthy/diseased donors with their informed consent (Department of Clinical Dermatology and Venereology, University Hospital, Lund, Sweden).

Mannan-Induced PsA. Mice were injected i.p. with 10 or 20 mg of mannan from the yeast *S. cerevisiae* (M7504, batch nos. 109K3780V and 061M7355; Sigma–Aldrich) dissolved in 200 μL of PBS, either only on day 0 or for multiple exposures additionally on days 7 and 14. Mice were scored daily for inflammation in the peripheral joints as described previously (59). The severity and incidence of the Ps-like skin manifestations were monitored on a scale ranging from 1 to 3 per mouse based on the severity of skin scaling on the paws: 1, weak skin peeling; 2, moderate skin peeling; and 3, heavy skin peeling with some hair loss.

Histological Evaluation. Naive and diseased mouse paws and healthy and psoriatic/eczematic skin biopsies were fixed in 4% paraformaldehyde (HistoLab Products AB), decalcified (only mouse paws), and embedded in paraffin. The ear tissue was frozen and embedded in Tissue Tec medium (Sakura Finetek Europe B.V.), and 10-μm sections were stained with H&E for the assessment of inflammation. For the evaluation of arthritis activity and severity in the ankle joint sections, the following histopathological scoring protocol was used: 1, mild synovitis with hyperplastic synovial membrane, small focal infiltration of inflammatory cells, and increased numbers of vessels in the synovium with no bone or cartilage erosions; 2, moderate synovitis, entheseal inflammation, cartilage erosions, and undisrupted joint architecture; and 3, severe pannus formation with extensive erosions of bone and cartilage and disrupted joint architecture.

Processing of Epidermal and Dermal Cells from Mouse Ears. Skin sheets from the naive and diseased mouse ears were separated from cartilage and processed as described earlier (60). Epidermal and dermal single-cell suspensions were subjected to flow cytometric analyses.

Induction of Monocyte/Macrophage Depletion in Vivo. CLs and the control liposomes (23) were purchased from Encapsula NanoSciences. A dose of 200 μL was administered i.v. on day −2 (premannan injection) and days +2 and +4 (postmannan injection).

Neutrophil Depletion in Vivo. For neutrophil depletion, 10-wk-old B10Q. *Ncf1*$^{m1j/m1j}$ male mice were treated with either anti-Ly6G (RB6-8C5) or the corresponding isotype control antibody (clone LTF-2) from BioXcell. A dose of 100 μg per 200 μL was administered i.v. on day −2 (premannan injection) and days +2 and +4 (postmannan injection).

Cytokine Neutralization in Vivo. Sex- and age-matched B10Q.*Ncf1*$^{m1j/m1j}$ mice were treated with either anti-mouse (anti-m) neutralizing antibodies or the isotype control antibodies (BioXcell): anti–mIL-17A (17F3), isotype control-mouse IgG1 (MOPC-21); anti–mIL-1β (B122), isotype control-polyclonal hamster IgG; anti–mTNF-α (TN3-19.12), isotype control-polyclonal hamster IgG; and anti–mIL-6 (MP5-20F3), isotype control-rat IgG1. For IL-17A neutralization, mice were injected with 100-μg doses i.v. on day −2 (premannan injection) and days +2, +4, and +6 (postmannan injection); however, for mIL-1β, mTNF-α, and IL-6 neutralization, antibodies were transferred only on days −2 +2, and +4.

Peritoneal and Skin Cell Culture. Anti-CD3 (1 μg/mL)- and anti-CD28 (5 μg/mL)-coated sterile culture plates were loaded with 0.5×10^6 peritoneal/skin cells in complete RPMI-1640 medium supplemented with different recombinant cytokines: IL-1β (50 ng/mL), IL-6 (50 ng/mL), IL-10 (10 ng/mL), IL-12 (10 ng/mL), IL-23 (50 ng/mL), and TNF-α (10 ng/mL). After 72 h of incubation at 37 °C, culture supernatant was collected and IL-17A levels were measured using a standard ELISA method as described below.

ELISA. IL-17A levels from culture supernatant were determined by ELISA using IL-17A capture antibody and bio–IL-17A detection antibodies (eBioscience). Binding of antibodies was detected by europium-labeled streptavidin using the dissociation-enhanced lanthanide fluoroimmunoassay system (Wallac). Results are expressed as fold change compared with naive mice.

Cytometric Bead Array. Cytokine levels in the skin culture supernatant were measured by flow cytometry using the eBioscience CBA mouse Th1/Th2 10plex kit (IL-1α, IL-2, IL-5, IL-6, IL-10, IFN-γ, TNF-α, GM-CSF, IL-4, and IL-17; BMS820FF) according to the manufacturer's instructions. Briefly, 1×10^6 skin cells were isolated from the naive and mannan-injected B10Q.$Ncf1^{m1j/m1j}$ mouse ear tissues and stimulated with phorbol 12-myristate 13-acetate (PMA)/ionomycin for 4 h at 37 °C. Cytokine concentrations were expressed as picograms per milliliter. Data were analyzed using Flowcytomix-Pro-3.0 (eBioscience).

Flow Cytometry Analysis. Single-cell suspensions from peripheral blood, PECs, and skin cells (1×10^6 cells) were labeled with the following monoclonal antibodies and analyzed using a Becton Dickinson FACSCalibur or LSR II: anti-CD11b-FITC/Pacific blue (M1/70), anti-Gr1-allophycocyanin (APC) (RB6-8C5), anti-CD11c-APC (N418), anti-Ly6G-phycoerythrin (PE) (1A8, RB6-8C5), anti-IL-17A-Alexa Fluor 647 (TC11-18H10.1), anti-γδ TCR-PE (GL3), anti-βTCR-peridinin chlorophyll (PerCP)-Cy5.5/FITC (H57-597), anti-F4/80-FITC/PerCP-Cy5.5 (BM8), anti-TNF-α-PE.Cy7 (TN3-19), anti-CCR6-PE.Cy7 (29-2L17), anti-TLR2 (CD282)-FITC (clone T2.5), and anti-CD45-PE-Cy7/APC/bio (30-F11). All of these antibodies were sourced either from Becton Dickinson, eBioscience, or Biolegend.

For intracellular cytokine staining, 1×10^6 peritoneal cells were stimulated in vitro in complete RPMI-1640 medium supplemented with 50 ng/mL PMA and 1 μM of ionomycin, and incubated for 2 h at 37 °C. For skin cells, 1×10^6 epidermis/dermis cells were stimulated in vitro in complete RPMI-1640 medium supplemented with 100 ng/mL PMA and 1 μM of ionomycin, and incubated for 4 h at 37 °C. Brefeldin A (10 μg/mL) was added to all of the samples from the start of the cultures, followed by permeabilization (eBioscience) and intracellular staining. Samples were analyzed using a FACS LSR II and FlowJo software (TreeStar, Inc.).

ROS Measurement in Vivo, L-012 Imaging. Mice were anesthetized and injected i.p. with 20 mg/kg of L-012 probe [8-amino-5-chloro-7-phenylpyrido (3,4-d) pyridazine-1,4 (2H,3H) dione] (21). Luminescent signals were detected using an IVIS 50 bioluminescent system (Xenogen). Image acquisition and analysis were performed using Living Image software (Xenogen).

In Vitro Intracellular Oxidative Burst. RBCs were lysed from heparinized blood with hypotonic lysis buffer, and leukocytes were stained with eFluor 450-conjugated anti-CD11b (M1/70) antibody (eBioscience) and PE-Cy7-conju-gated anti-Ly6G antibody (BD Pharmingen). Cells were suspended in HBSS and incubated for 10 min at 37 °C with 3 μM DHR-123 (Molecular Probes and Invitrogen Life Technologies). Normal mouse serum from B10Q mice diluted 1:2 in HBSS was used in indicated samples. The cells were incubated for 3 h at 37 °C with 1 mg/mL mannan or 1 mg/mL zymosan (Sigma), or without any stimulant. After oxidation by ROS, DHR-123 emits fluorescence upon excitation with a blue laser. The cells were washed with PBS and acquired on an LSR II flow cytometer equipped with FACS Diva software (BD Biosciences). Live cells were gated on the cell type, and geometric means of respective populations were analyzed using Flowing Software (Cell Imaging Core, University of Turku).

Mouse Skin Tissue Immunofluorescence Staining Analysis. Formalin-fixed, paraffin-embedded mouse ear/paw skin tissue sections were first depar-affinized in xylene (2 × 5 min), hydrated with ethanol (99% for 2 × 3 min, 95% for 1 min), and rinsed in distilled water. Sections were then pretreated with trypsin for epitope unmasking (30 min at 37 °C) and washed. For staining with MECA-79 (MECA-79 is expressed on high endothelial venules of lymphoid tissues, chronically inflamed tissues, and rheumatoid synovia), sections were incubated with anti-human/mouse MECA-79 Alexa Fluor 488 (53-6036-80; Affymetrix eBioscience) at a 1:50 dilution for 45 min. For the staining with involucrin, rat serum and avidin-biotin blocking were used before the addition of purified anti-mouse involucrin antibody (1:25 dilution). As a secondary reagent, biotin-conjugated anti-IgG1 was added, followed by streptavidin-Cy3 for visualization. All of the incubation steps with antibodies were performed at room temperature, and all of the washing steps were done using PBS-Tween buffer (3 × 3 min).

Statistics. The Mann–Whitney U test was performed for comparison of two unpaired nonparametric sample groups. GraphPad Prism software, version 5.0c, or SigmaPlot was used for statistical analysis. $P < 0.05$ was considered as significant.

1. Nickoloff BJ, Nestle FO (2004) Recent insights into the immunopathogenesis of psoriasis provide new therapeutic opportunities. *J Clin Invest* 113(12):1664–1675.
2. Liu Y, et al. (2008) A genome-wide association study of psoriasis and psoriatic arthritis identifies new disease loci. *PLoS Genet* 4(3):e1000041.
3. Tsoi LC, et al.; Collaborative Association Study of Psoriasis (CASP); Genetic Analysis of Psoriasis Consortium; Psoriasis Association Genetics Extension; Wellcome Trust Case Control Consortium 2 (2012) Identification of 15 new psoriasis susceptibility loci highlights the role of innate immunity. *Nat Genet* 44(12):1341–1348.
4. Knight J, et al.; Wellcome Trust Case Control Consortium; Genetic Analysis of Psoriasis Consortium; I-chip for Psoriasis Consortium (2012) Conditional analysis identifies three novel major histocompatibility complex loci associated with psoriasis. *Hum Mol Genet* 21(23):5185–5192.
5. Gladman DD, Farewell VT (2003) HLA studies in psoriatic arthritis: Current situation and future needs. *J Rheumatol* 30(1):4–6.
6. Griffiths CE, Barker JN (2007) Pathogenesis and clinical features of psoriasis. *Lancet* 370(9583):263–271.
7. Picciani BL, et al. (2013) Oral candidiasis in patients with psoriasis: Correlation of oral examination and cytopathological evaluation with psoriasis disease severity and treatment. *J Am Acad Dermatol* 68(6):986–991.
8. Bernotiene E, et al. (2004) Delayed resolution of acute inflammation during zymosan-induced arthritis in leptin-deficient mice. *Arthritis Res Ther* 6(3):R256–R263.
9. van der Fits L, et al. (2009) Imiquimod-induced psoriasis-like skin inflammation in mice is mediated via the IL-23/IL-17 axis. *J Immunol* 182(9):5836–5845.
10. Kumari S, et al. (2013) Tumor necrosis factor receptor signaling in keratinocytes triggers interleukin-24-dependent psoriasis-like skin inflammation in mice. *Immunity* 39(5):899–911.
11. Maeda S, Hayami Y, Naniwa T, Ueda R (2012) The Th17/IL-23 Axis and Natural Immunity in Psoriatic Arthritis. *Int J Rheumatol* 2012:539683.
12. Ueyama A, et al. (2014) Mechanism of pathogenesis of imiquimod-induced skin inflammation in the mouse: A role for interferon-alpha in dendritic cell activation by imiquimod. *J Dermatol* 41(2):135–143.
13. Nishimoto S, et al. (2013) Th17 cells carrying TCR recognizing epidermal autoantigen induce psoriasis-like skin inflammation. *J Immunol* 191(6):3065–3072.
14. Ariza ME, Williams MV, Wong HK (2013) Targeting IL-17 in psoriasis: From cutaneous immunobiology to clinical application. *Clin Immunol* 146(2):131–139.
15. Hultqvist M, et al. (2004) Enhanced autoimmunity, arthritis, and encephalomyelitis in mice with a reduced oxidative burst due to a mutation in the Ncf1 gene. *Proc Natl Acad Sci USA* 101(34):12646–12651.
16. Sareila O, Kelkka T, Pizzolla A, Hultqvist M, Holmdahl R (2011) NOX2 complex-derived ROS as immune regulators. *Antioxid Redox Signal* 15(8):2197–2208.
17. Holmdahl R, et al. (2013) Hydrogen peroxide as an immunological transmitter regulating autoreactive T cells. *Antioxid Redox Signal* 18(12):1463–1474.
18. Sareila O, Jaakkola N, Olofsson P, Kelkka T, Holmdahl R (2013) Identification of a region in p47phox/NCF1 crucial for phagocytic NADPH oxidase (NOX2) activation. *J Leukoc Biol* 93(3):427–435.
19. Raychaudhuri SP, Jiang WY, Raychaudhuri SK (2008) Revisiting the Koebner phenomenon: Role of NGF and its receptor system in the pathogenesis of psoriasis. *Am J Pathol* 172(4):961–971.
20. Forsberg E, et al. (1999) Abnormal mast cells in mice deficient in a heparin-synthe-sizing enzyme. *Nature* 400(6746):773–776.
21. Kelkka T, Hultqvist M, Nandakumar KS, Holmdahl R (2012) Enhancement of antibody-induced arthritis via Toll-like receptor 2 stimulation is regulated by granulocyte reactive oxygen species. *Am J Pathol* 181(1):141–150.
22. Gelderman KA, et al. (2007) Macrophages suppress T cell responses and arthritis development in mice by producing reactive oxygen species. *J Clin Invest* 117(10):3020–3028.
23. Chamberlain CS, et al. (2011) The influence of macrophage depletion on ligament healing. *Connect Tissue Res* 52(3):203–211.
24. Kagami S, Rizzo HL, Kurtz SE, Miller LS, Blauvelt A (2010) IL-23 and IL-17A, but not IL-12 and IL-22, are required for optimal skin host defense against Candida albicans. *J Immunol* 185(9):5453–5462.
25. Ryan C, Abramson A, Patel M, Menter A (2012) Current investigational drugs in psoriasis. *Expert Opin Investig Drugs* 21(4):473–487.
26. Zenz R, et al. (2005) Psoriasis-like skin disease and arthritis caused by inducible epidermal deletion of Jun proteins. *Nature* 437(7057):369–375.
27. Bárdos T, Zhang J, Mikecz K, David CS, Glant TT (2002) Mice lacking endogenous major histocompatibility complex class II develop arthritis resembling psoriatic arthritis at an advanced age. *Arthritis Rheum* 46(9):2465–2475.
28. Wang H, et al. (2008) A 9-centimorgan interval of chromosome 10 controls the T cell-dependent psoriasiform skin disease and arthritis in a murine psoriasis model. *J Immunol* 180(8):5520–5529.

29. Gilliet M, et al. (2004) Psoriasis triggered by toll-like receptor 7 agonist imiquimod in the presence of dermal plasmacytoid dendritic cell precursors. *Arch Dermatol* 140(12): 1490–1495.

30. Wang H, et al. (2010) Extracellular adherence protein of Staphylococcus aureus suppresses disease by inhibiting T-cell recruitment in a mouse model of psoriasis. *J Invest Dermatol* 130(3):743–754.

31. Mease PJ (2011) Psoriatic arthritis: Update on pathophysiology, assessment and management. *Ann Rheum Dis* 70(Suppl 1):i77–i84.

32. Sagi L, Trau H (2011) The Koebner phenomenon. *Clin Dermatol* 29(2):231–236.

33. Zhou Q, Mrowietz U, Rostami-Yazdi M (2009) Oxidative stress in the pathogenesis of psoriasis. *Free Radic Biol Med* 47(7):891–905.

34. Foerster J, et al. (2006) Neutrophil respiratory burst is decreased in scleroderma and normalized by near-infrared mediated hyperthermia. *Clin Exp Dermatol* 31(6): 799–806.

35. Kim HR, et al. (2014) Reactive oxygen species prevent imiquimod-induced psoriatic dermatitis through enhancing regulatory T cell function. *PLoS ONE* 9(3):e91146.

36. Olsson LM, et al. (2007) A case-control study of rheumatoid arthritis identifies an associated single nucleotide polymorphism in the NCF4 gene, supporting a role for the NADPH-oxidase complex in autoimmunity. *Arthritis Res Ther* 9(5):R98.

37. Deffert C, et al. (2012) Hyperinflammation of chronic granulomatous disease is abolished by NOX2 reconstitution in macrophages and dendritic cells. *J Pathol* 228(3): 341–350.

38. Hueber AJ, McInnes IB (2007) Immune regulation in psoriasis and psoriatic arthritis—Recent developments. *Immunol Lett* 114(2):59–65.

39. Ackermann L, et al. (1999) Mast cells in psoriatic skin are strongly positive for interferon-gamma. *Br J Dermatol* 140(4):624–633.

40. Wang Y, Rollins SA, Madri JA, Matis LA (1995) Anti-C5 monoclonal antibody therapy prevents collagen-induced arthritis and ameliorates established disease. *Proc Natl Acad Sci USA* 92(19):8955–8959.

41. Rosenberg EW, Noah PW, Wyatt RJ, Jones RM, Kolb WP (1990) Complement activation in psoriasis. *Clin Exp Dermatol* 15(1):16–20.

42. Stratis A, et al. (2006) Pathogenic role for skin macrophages in a mouse model of keratinocyte-induced psoriasis-like skin inflammation. *J Clin Invest* 116(8):2094–2104.

43. Wang H, et al. (2006) Activated macrophages are essential in a murine model for T cell-mediated chronic psoriasiform skin inflammation. *J Clin Invest* 116(8):2105–2114.

44. Song C, et al. (2008) IL-17-producing alveolar macrophages mediate allergic lung inflammation related to asthma. *J Immunol* 181(9):6117–6124.

45. Hashimoto M, et al. (2010) Complement drives Th17 cell differentiation and triggers autoimmune arthritis. *J Exp Med* 207(6):1135–1143.

46. Pantelyushin S, et al. (2012) Rorγt+ innate lymphocytes and γδ T cells initiate psoriasiform plaque formation in mice. *J Clin Invest* 122(6):2252–2256.

47. Garber K (2012) Anti-IL-17 mAbs herald new options in psoriasis. *Nat Biotechnol* 30(6): 475–477.

48. Jouault T, et al. (2006) Specific recognition of Candida albicans by macrophages requires galectin-3 to discriminate Saccharomyces cerevisiae and needs association with TLR2 for signaling. *J Immunol* 177(7):4679–4687.

49. Nograles KE, et al. (2008) Th17 cytokines interleukin (IL)-17 and IL-22 modulate distinct inflammatory and keratinocyte-response pathways. *Br J Dermatol* 159(5): 1092–1102.

50. Homey B, et al. (2000) Up-regulation of macrophage inflammatory protein-3 alpha/CCL20 and CC chemokine receptor 6 in psoriasis. *J Immunol* 164(12):6621–6632.

51. Harper EG, et al. (2009) Th17 cytokines stimulate CCL20 expression in keratinocytes in vitro and in vivo: Implications for psoriasis pathogenesis. *J Invest Dermatol* 129(9): 2175–2183.

52. Hedrick MN, et al. (2009) CCR6 is required for IL-23-induced psoriasis-like inflammation in mice. *J Clin Invest* 119(8):2317–2329.

53. Laggner U, et al. (2011) Identification of a novel proinflammatory human skin-homing Vγ9Vδ2 T cell subset with a potential role in psoriasis. *J Immunol* 187(5): 2783–2793.

54. Girardi M (2006) Immunosurveillance and immunoregulation by gammadelta T cells. *J Invest Dermatol* 126(1):25–31.

55. Mease PJ, et al. (2010) Patient-reported outcomes in a randomized trial of etanercept in psoriatic arthritis. *J Rheumatol* 37(6):1221–1227.

56. Ikeda S, et al. (2013) Therapeutic depletion of myeloid lineage leukocytes in patients with generalized pustular psoriasis indicates a major role for neutrophils in the immunopathogenesis of psoriasis. *J Am Acad Dermatol* 68(4):609–617.

57. Pizzolla A, et al. (2012) Reactive oxygen species produced by the NADPH oxidase 2 complex in monocytes protect mice from bacterial infections. *J Immunol* 188(10): 5003–5011.

58. Lindqvist AK, et al. (2006) Backcross and partial advanced intercross analysis of nonobese diabetic gene-mediated effects on collagen-induced arthritis reveals an interactive effect by two major loci. *J Immunol* 177(6):3952–3959.

59. Holmdahl RCS, et al. (1998) Genetic analysis of murine models for rheumatoid arthritis. *Human Genome Methods*, ed Adolpho K (CRC, New York):pp 215–238.

60. Mabuchi T, et al. (2013) CCR6 is required for epidermal trafficking of γδ-T cells in an IL-23-induced model of psoriasiform dermatitis. *J Invest Dermatol* 133(1):164–171.

Khmaladze et al.